http://dx.doi.org/10.7567/JJAP.53.07KF17

Measurement of shear viscoelasticity using dual acoustic radiation pressure induced by continuous-wave ultrasounds

Kaori Tachi[1], Hideyuki Hasegawa[1,2], and Hiroshi Kanai[1,2*]

[1]*Graduate School of Biomedical Engineering, Tohoku University, Sendai 980-8579, Japan*
[2]*Graduate School of Engineering, Tohoku University, Sendai 980-8579, Japan*
E-mail: kanai@ecei.tohoku.ac.jp

Received November 29, 2013; revised January 31, 2014; accepted February 13, 2014; published online June 19, 2014

It is important to evaluate the viscoelasticity of muscle for assessment of its condition. However, quantitative and noninvasive diagnostic methods have not yet been established. In our previous study, we developed a method, which used ultrasonic acoustic radiation forces irradiated from two opposite horizontal directions, for measurement of the viscoelasticity. Using two continuous wave ultrasounds, an object can be actuated with an ultrasonic intensity, which is far lower (0.9 W/cm^2) than that in the case of the conventional acoustic radiation force impulse (ARFI) method. In the present study, in vitro experiments using phantoms made of polyurethane rubber and porcine muscle tissue embedded in a gelatin block were conducted. We actuated phantoms by ultrasonic radiation force and measured the propagation velocity of the generated shear wave inside the phantoms using a diagnostic ultrasound system. The viscoelasticities of phantoms were estimated by fitting a viscoelastic model, i.e., the Voigt model, to the frequency characteristic of the measured shear wave propagation speed. In the mechanical tensile test, a softer polyurethane phantom exhibited a lower elasticity and a higher viscosity than a polyurethane phantom with a higher elasticity and a lower viscosity. The viscoelasticity measured by ultrasound showed the same tendency as that in the tensile test. Furthermore, the viscoelasticity of the phantom with porcine muscular tissue was measured in vitro, and the estimated viscoelasticity agreed well with that reported in the literature. These results show the possibility of the proposed method for noninvasive and quantitative assessment of the viscoelasticity of biological soft tissue.

1. Introduction

Viscoelastic properties of muscle tissue are closely related to the pathological state. For example, owing to pyramidal tract disorders or peripheral neuropathy, the elastic modulus of muscle decreases. In amyloidosis, atrophy and elevation of the hardness of muscle occur. Also, polymyositis and myoglobinuria lead to muscle weakness (decrease in muscle elasticity).[1,2] Therefore, it would be valuable to measure the viscoelasticity of muscle for early detection and quantitative diagnosis of muscle disorder.

Over the past decade, some remote actuation methods based on acoustic radiation forces have been reported. Fatemi and coworkers proposed an imaging modality that uses the acoustic responses of an object, which are closely related to the mechanical properties of the medium. By measuring the acoustic emission with a hydrophone, hard inclusions, such as calcified tissues in soft materials, were detected experimentally.[3,4] However, the spatial resolution was limited by the size of the intersectional area of ultrasound beams at two slightly different frequencies.

Nightingale and coworkers proposed an alternative imaging method (acoustic radiation force impulse: ARFI), in which focused ultrasound is employed to apply a radiation force to soft tissue for a short duration (less than 1 ms). The viscoelastic properties of the tissue were investigated from the magnitude of the transient response, which was measured with ultrasound as the displacement of tissue.[5–7] However, in order to generate a measurable displacement by several ultrasonic pulses, high-intensity pulsed ultrasound at 1,000 W/cm^2 was required. According to safety guidelines for the use of diagnostic ultrasound, it is recommended that the intensity be below 240 mW/cm^2 (I_{SPTA}) for pulsed waves and 1 W/cm^2 for continuous waves.[8] The intensity of the pulsed ultrasound employed by Nightingale and coworkers was therefore far greater than that indicated by the safety guidelines. Later many groups studied methods for actuation using high-intensity pulsed ultrasound and the measurement of viscoelastic properties of tissue.[9,10]

To decrease the ultrasonic intensity for actuation of soft tissue, we chose continuous-wave ultrasound, as in the work carried out by Fatemi and coworkers. The maximum intensity of 1 W/cm^2 for continuous waves given by the safety guidelines generates an acoustic radiation force of 6.67 Pa, which is very small. Therefore, to generate a measurable displacement by acoustic actuation, a method for effective application of acoustic radiation forces should be developed. However, a single acoustic radiation force does not generate deformation in an object effectively because it primarily produces a change in object's position. In our previous study, we developed a method, in which two cyclical radiation forces were simultaneously applied to a phantom from two opposite horizontal directions to cyclically compress the object in the horizontal direction. Furthermore, the resultant regional displacement and strain in the tissue were measured using a different ultrasonic probe. This method enables the effective generation of deformation by acoustic actuation.[11,12]

There is another study using two sources of shear waves,[13] in which a method for evaluating the mechanical properties of an object by making two shear waves interfere with each other is presented. However, this method requires that two shear wave sources are perfectly opposite, and that shear waves are insonified from the skin surface by an external vibrator. On the other hand, our method does not have these requirements. Also, the shear wave sources (corresponding to focal spots of two ultrasonic transducers) can be placed inside an object and can be localized using focused transducers.

In the present study, the propagation of the shear wave generated by our ultrasonic actuation method was measured also by ultrasound to evaluate the viscoelastic properties of an object.

2. Materials and methods

2.1 Acoustic radiation pressure at frequency difference of two continuous ultrasounds

When the ultrasound at a single frequency propagates in a medium, a constant force is generated in the direction of propagation. This force is called the acoustic radiation force. The acoustic radiation pressure is defined as the acoustic radiation force per unit area.[14] When inserting an object (density ρ_2, sound speed c_2) in the medium (density ρ_1, sound speed c_1), the ultrasound wave, which is incident perpendicularly on the surface of the object and progressing in the object, is given by Euler's fluid motion equation:[15]

$$\frac{\partial v(z,t)}{\partial t} + v(z,t)\frac{\partial v(z,t)}{\partial z} = -\frac{1}{\rho_2}\frac{\partial p(z,t)}{\partial z}, \tag{1}$$

where $v(z,t)$ and $p(z,t)$ are the particle velocity and the sound pressure in an object, respectively. Equation (1) is modified to

$$\rho_2\frac{\partial v(z,t)}{\partial t} + \frac{\partial}{\partial z}\frac{1}{2}\rho_2 v^2(z,t) = -\frac{\partial p(z,t)}{\partial z}, \tag{2}$$

where $\rho_2 \partial v(z,t)/\partial t$ and $\rho_2 v^2(z,t)/2$ correspond to the acoustic radiation pressure and the kinetic energy of the ultrasound, respectively. Therefore, the acoustic radiation pressure is given by

$$P_R(z,t) = -\frac{\partial}{\partial z}(e(z,t) + p(z,t)). \tag{3}$$

When two ultrasounds with the same sound pressure, p_0, at slightly different frequencies, f_0 and $(f_0 + \Delta f)$, cross each other, an acoustic radiation pressure which fluctuates at the frequency difference, Δf, is generated in the intersectional space. The sound pressure, $p_{sum}(t)$, in the intersectional space is given by

$$\begin{aligned} p(z,t) = e^{-\alpha\cdot z}[&p_0\cos(kz - 2\pi f_0 t) \\ &+ p_0\cos\{kz - 2\pi(f_0+\Delta f)t\}], \end{aligned} \tag{4}$$

where α and k are the attenuation coefficient and the wave number, respectively. The kinetic energy $e(z,t)$ is expressed as

$$e(z,t) = \frac{1}{2}\rho_2 v^2(z,t) = \frac{1}{2}\rho_2\left(\frac{p(z,t)}{\rho_2 c_2}\right)^2 = \frac{1}{2\rho_2 c_2^2}p^2(z,t). \tag{5}$$

Therefore, the following equation is obtained from Eqs. (3)–(5).

$$\begin{aligned} P_R(z,t) = &-\frac{\partial}{\partial z}\Bigg(\frac{1}{2\rho_2 c_2^2}e^{-\alpha\cdot z}[p_0\cos(kz - 2\pi f_0 t) \\ &+ p_0\cos\{kz - 2\pi(f_0+\Delta f)t\}]^2 \\ &+ [p_0\cos(kz - 2\pi f_0 t) \\ &+ p_0\cos\{kz - 2\pi(f_0+\Delta f)t\}]\Bigg) \\ = &\frac{\alpha p_0^2}{\rho_2 c_2^2}e^{-2\alpha\cdot z}(1 + \cos 2\pi\Delta f t) \\ &+ \frac{\alpha p_0^2}{2\rho_2 c_2^2}e^{-2\alpha\cdot z}[\cos 2(kz - 2\pi f_0 t) \\ &+ \cos\{2kz - 2\pi(f_0+\Delta f)t\} \\ &+ 2\cos\{2kz - 2\pi(2f_0+\Delta f)t\}] \\ &+ \frac{kp_0^2}{2\rho_2 c_2^2}e^{-2\alpha\cdot z}[\sin 2(kz - 2\pi f_0 t) \\ &+ \sin 2\{kz - 2\pi(f_0+\Delta f)t\} \\ &+ 2\sin(2kz - 2\pi(2f_0+\Delta f)t)] \\ &- p_0 e^{-\alpha\cdot z}[\alpha\cos(kz - 2\pi f_0 t) \\ &+ \alpha\cos\{kz - 2\pi(f_0+\Delta f)t\} + k\sin(kz - 2\pi f_0 t) \\ &+ k\sin\{kz - 2\pi(f_0+\Delta f)t\}]. \end{aligned} \tag{6}$$

Since the displacement of the object generated by the high-frequency component is negligible because it is sufficiently smaller than that generated by the low-frequency components at DC and Δf, the acoustic radiation pressure $P_R(z,t)$ is approximately given by

$$P_R(z,t) \approx \frac{\alpha p_0^2}{\rho_2 c_2^2}e^{-2\alpha\cdot z}(1 + \cos 2\pi\Delta f t). \tag{7}$$

2.2 Estimation of shear modulus from propagation velocity of shear wave using viscoelastic model of medium

When acoustic radiation pressures are applied to an object, a shear wave is generated and propagates. The shear modulus G is estimated from the measurement of the shear wave propagation speed c_s expressed as

$$G = \rho c_s^2, \tag{8}$$

where ρ is the density in the object.

To determine the shear wave propagation speed c_s, displacements of the object produced by acoustic radiation forces were measured also with ultrasound at multiple points along the propagation path of the shear wave. From the measured displacements, the shear wave propagation speed c_s is estimated as

$$c_s = \frac{2\pi\Delta f\Delta l}{\Delta\theta}, \tag{9}$$

where Δl and $\Delta\theta$ are the interval of ultrasonic beams for measurement and the phase difference between displacements of the object measured in neighboring ultrasonic beams, as illustrated in Fig. 1, respectively.

On the basis of Eq. (8), only the shear modulus can be estimated from the shear wave propagation speed. In the present study, the viscoelastic properties of an object were estimated as described below: The propagation of the shear wave is expressed by the wave equation as[16]

$$\frac{\partial^2 U}{\partial x^2} + k^2 U = 0, \tag{10}$$

$$c_s = \frac{\omega}{Re(k)}, \tag{11}$$

where U, k, and ω are the temporal Fourier transform of displacement, wave number, and angular frequency, respectively. When the Voigt model is used as a viscoelastic model of an object, the shear wave velocity is modeled as[17]

$$c_s = \sqrt{\frac{2(\mu_1^2 + \omega^2\mu_2^2)}{\rho(\mu_1 + \sqrt{\mu_1^2 + \omega^2\mu_2^2})}}, \tag{12}$$

where ρ, μ_1, and μ_2 are the density of an object, shear elasticity, and shear viscosity, respectively.

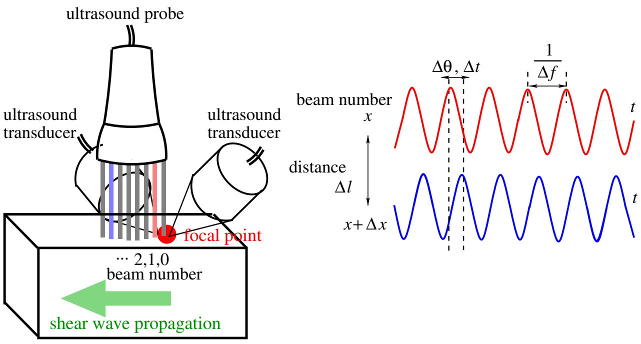

Fig. 1. (Color online) Schematic diagram of the method of estimating shear wave propagation speed.

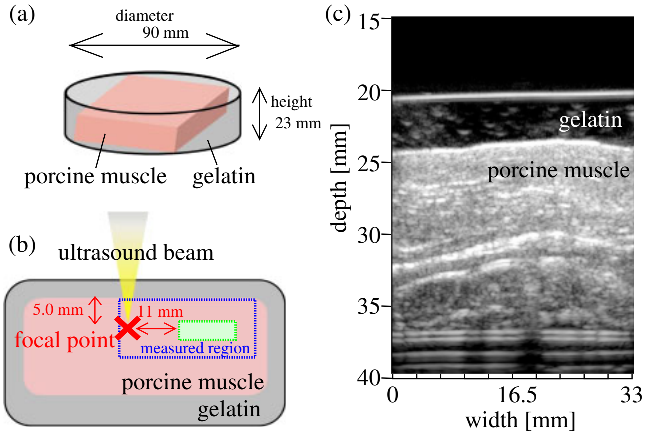

Fig. 3. (Color online) Illustration of porcine muscle phantom.

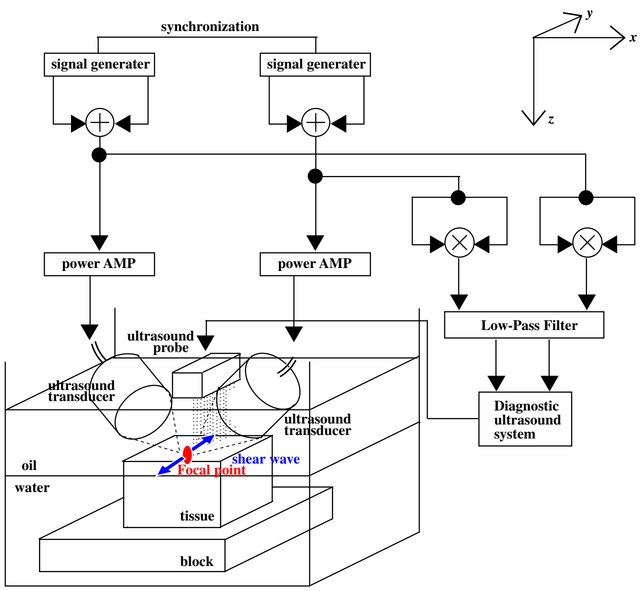

Fig. 2. (Color online) Schematic diagram of the experimental setup.

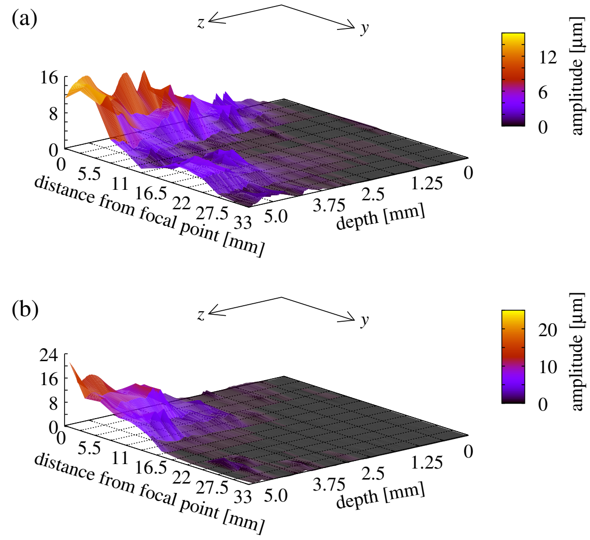

Fig. 4. (Color online) Spatial distributions of amplitudes of displacements at Δf of 5 Hz estimated by the Fourier transform. The results were obtained for phantoms of ASKER C hardnesses with (a) 0 and (b) 5.

2.3 Experimental methods

Figure 2 shows a schematic diagram of the experimental system. To measure the displacement distribution at a high spatial resolution, we employed ultrasonic diagnostic equipment (Hitachi-Aloka ProSound F75) with a 10 MHz linear probe (Hitachi-Aloka UST-5415). The frame rate and interval between ultrasonic beams were set at 486 Hz and 2.75 mm, respectively. The number of beams used in the measurement was 13 (beam number: 0–12). As shown in Fig. 1, the 0-th beam was located at the center of the two ultrasonic focal points for actuation.

To improve the spatial resolution in the measurement of the response of an object to the acoustic radiation force, an ultrasound correlation-based method, the *phased-tracking method*,[18,19] was used to measure the distribution of minute displacements. The accuracy of the displacement measurement by the *phased-tracking method* has already been evaluated to be 0.2 μm by basic experiments using a rubber plate[20] and, also, has already been applied to measurements of vibrations and viscoelasticities of the arterial wall[21,22] and heart wall.[23,24]

We used two phantoms made of two different polyurethane rubbers that simulate soft biological tissues and another phantom containing porcine muscle tissue to measure the propagation of the shear wave and estimate the viscoelasticity. The dimensions of the two polyurethane rubber phantoms were 90 mm in diameter and 20 mm in height, and their hardnesses were determined to be 0 and 5 using the ASKER C-type durometer. The porcine muscle phantom used in the present study is illustrated in Fig. 3. As illustrated in Fig. 3, the phantom was obtained by embedding a porcine muscle tissue in gelatin to prevent the deterioration of the porcine muscle by immersing in water. The position of the measured region is indicated by the blue dashed line.

3. Experimental results and discussion

3.1 Basic experiments using polyurethane rubber phantoms

Figures 4(a) and 4(b) show the spatial distributions of displacements in polyurethane rubber phantoms with ASKER C hardnesses of 0 and 5, respectively, estimated at $\Delta f = 5$ Hz using the Fourier transform. Focal points of ultrasonic beams for actuation were set at a depth of approximately 5 mm. The intensity of each ultrasound for actuation was 0.9 W/cm^2. As can be seen in Fig. 4, the shear wave is attenuated in accordance with its distance from the focal point.

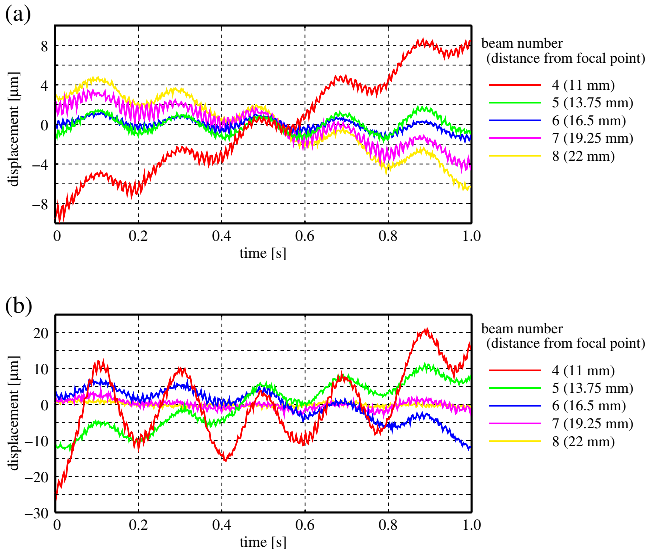

Fig. 5. (Color online) Displacements of polyurethane phantoms with ASKER C hardnesses of (a) 0 and (b) 5 at Δf of 5 Hz. Displacements were measured at (a) 5.5 and (b) 5.1 mm in depth.

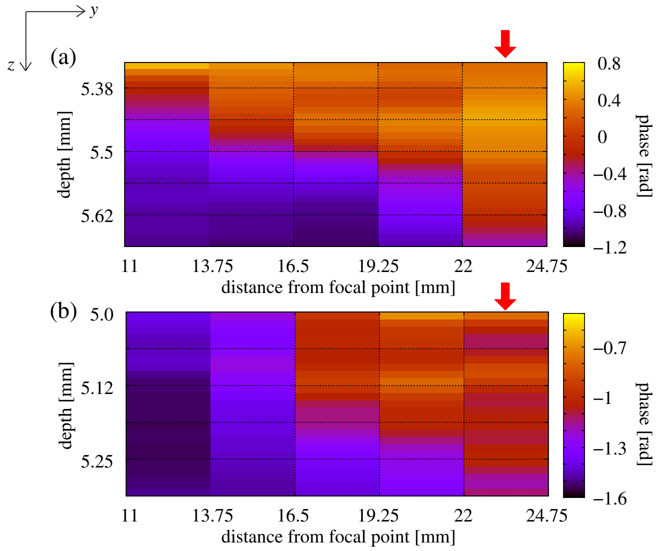

Fig. 6. (Color online) Spatial distributions of phases of displacements at Δf of 5 Hz obtained for phantoms with ASKER C hardnesses of (a) 0 and (b) 5.

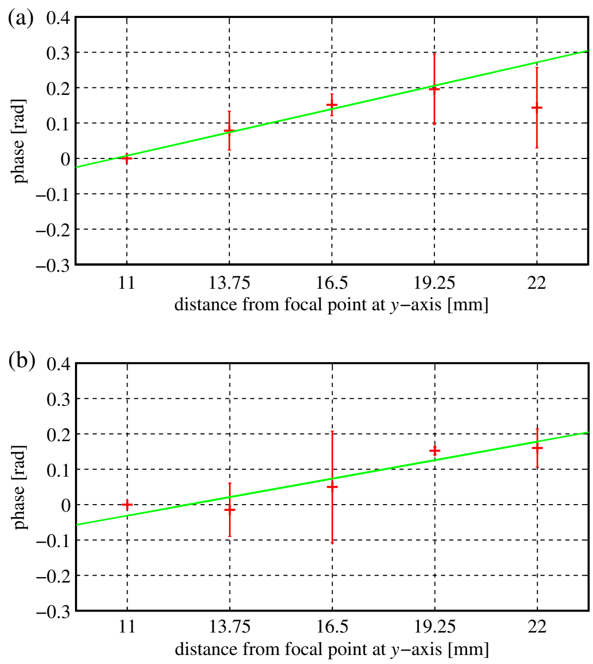

Fig. 7. (Color online) Averaged phases of displacements at Δf of 5 Hz plotted as functions of distance obtained for phantoms with ASKER C hardnesses of (a) 0 and (b) 5. The green lines show the regression lines determined by the least-squares method.

Figure 5 shows the displacement waveforms measured in the respective polyurethane rubber phantoms located 5.5 to 22 mm away from the focal point. The depths, where the displacements were measured, were (a) 5.5 and (b) 5.1 mm. It can be seen that the phase lag occurs between the waveforms in Fig. 5, which is caused by the wave propagation. For example, the peak of the waveform at beam number 4 (distance from the focal point is 11 mm) is formed slightly before that at beam number 5 (distance from focal point is 13.75 mm).

Figures 6(a) and 6(b) show spatial distributions of phases of displacements measured in the phantoms with ASKER C hardnesses of 0 and 5, respectively, estimated at $\Delta f = 5$ Hz using the Fourier transform. As shown in Fig. 6, it is confirmed that the phase increases with the distance, which is shown by the red arrow in the figure. Means and standard deviations of phases at Δf evaluated for three measurements are shown in Fig. 7. The depths, where the phases in Figs. 6(a) and 6(b) were estimated, were 5.5 and 5.1 mm, respectively. The phases were obtained as the values relative to the phase measured at beam number 4 (distance from focal point: 11 mm). From Fig. 7 and Eq. (9), it can be seen that the shear wave propagates in the direction away from the focal point. Shear wave velocities of polyurethane rubber phantoms with hardnesses of 0 and 5 were estimated to be 1.2 and 1.7 m/s, respectively, using Eq. (9) with the slopes corresponding to $\Delta\theta/\Delta l$ in Eq. (9) of the regression lines (green lines in Fig. 7) determined by the least-squares method. To discuss the accuracy of the estimated values, we measured the shear wave velocity of the polyurethane rubber phantom with an ASKER C hardness of 0 for three times. The mean and standard deviation were 1.76 and 0.06 m/s (at Δf of 5 Hz), respectively. Therefore, in the present paper, the number of digits after the decimal point was set at one. There is a relatively large variation in the estimated phase. The reason for the variation is not perfectly clear, but the generated displacement is very small and might be affected by an undesirable vibration from the environment. We need to clarify the reason for the variance and to develop a method for separating the displacement induced by acoustic radiation force from the environmental vibration because we aim to actuate an object within the maximal acoustic output suggested by the safety guideline.

The propagation velocities of shear waves in the phantoms with hardnesses of 0 and 5 are plotted as a function of Δf in Fig. 8. The measured frequency characteristics of shear wave propagation velocities fit well to those obtained using the Voigt model shown by Eq. (12). The estimated elastic moduli and viscosity constants of the phantoms with hardnesses of 0 and 5 were ($\mu_1^0 = 2.2$ kPa, $\mu_2^0 = 48.1$ Pa·s) and ($\mu_1^5 =$

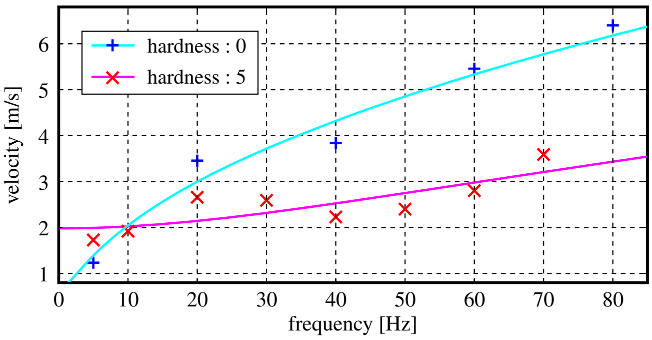

Fig. 8. (Color online) Shear wave propagation speeds in phantoms plotted as functions of Δf. The solid lines show the frequency characteristics obtained using the Voigt model.

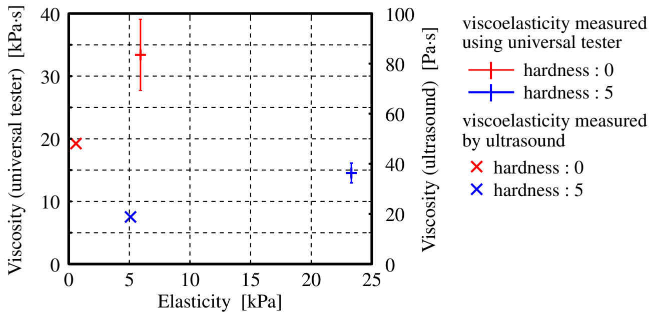

Fig. 10. (Color online) Comparison of viscoelastic constants of polyurethane phantoms measured using precision tensile tester with those measured by ultrasound.

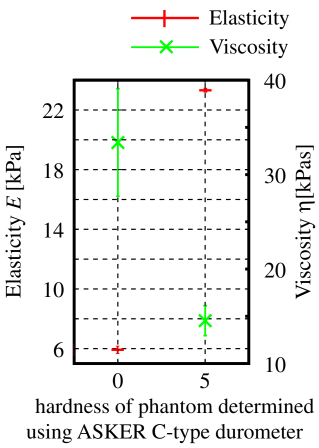

Fig. 9. (Color online) Viscoelastic constants of polyurethane phantoms measured using precision tensile tester.

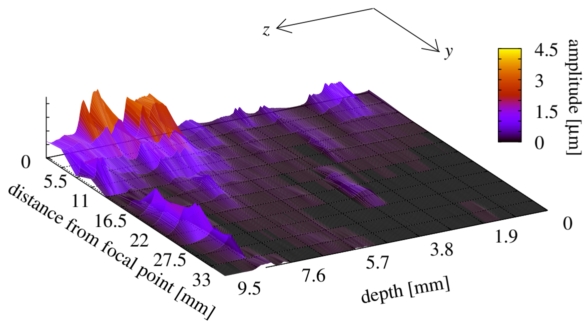

Fig. 11. (Color online) Spatial distribution of amplitudes of displacements at Δf of 5 Hz measured in porcine muscle phantom.

5.1 kPa, $\mu_2^5 = 18.8$ Pa·s), respectively. The root mean square difference (RMSE) between the measured values and the values estimated using the model shown in Fig. 8 was also evaluated. RMSEs with respect to phantoms with hardnesses of 0 and 5 were 7 and 13%, respectively.

Figure 9 shows the elastic moduli and viscosity constants of the respective phantoms measured using a precision universal tester (Shimadzu AG-X 10kN). In Fig. 9, plots and vertical bars show means and standard deviations for 10 measurements, respectively.

As shown in Fig. 9, viscoelastic properties of the polyurethane rubber phantoms estimated using the precision universal tester were ($\hat{\mu}_1^0 = 5.92 \pm 0.24$ kPa, $\hat{\mu}_2^0 = 33.40 \pm 5.68$ kPa·s) and ($\hat{\mu}_1^5 = 23.32 \pm 0.08$ kPa, $\hat{\mu}_2^5 = 14.54 \pm 1.58$ kPa·s).

There were significant differences between the absolute values obtained by ultrasound and those obtained using the precision universal tester. In the measurement using the universal tester, the actuation frequency was about 1 Hz, and the maximum strain in the object was about 20% due to limitations of the specifications of the tester. In general, the viscoelastic properties depend on the magnitude of strain, and the different levels of deformation may be one of the reasons for the differences in the absolute values of the viscoelastic constants. However, as shown in Fig. 10, similar tendencies of the viscoelastic constants (higher elastic modulus of the phantom with the hardness of 5 and higher viscosity constant of the phantom with the hardness of 0) were found in both measurements with ultrasound and the universal tester.

3.2 In vitro experiment using porcine muscle tissue

In the present study, an in vitro experiment using a gelatin phantom containing porcine abdominal muscle tissue was conducted to investigate whether the proposed method could generate and measure the presumed shear wave. Figure 11 shows the spatial distribution of amplitudes of displacements at $\Delta f = 5$ Hz estimated by applying the Fourier transform to displacement waveforms measured by ultrasound. The focal points of ultrasonic beams for actuation were set at a depth of approximately 5.7 mm.

Figure 12(a) shows the displacement waveforms measured at a depth of 5.7 mm in the porcine muscle at $\Delta f = 5$ Hz. The spatial distribution of phases of the measured displacement waveforms is shown in Fig. 12(b), and the averaged phase at Δf of 5 Hz is shown in Fig. 12(c), where plots and vertical bars show means and standard deviations, respectively. In Fig. 12(a), a frequency component of about 100 Hz is clearly seen. The amplitude of this component increases when the acoustic radiation force increases (corresponding to the downward displacement of the object). Therefore, this component might be the high-frequency component of the acoustic radiation force, which was neglected in the present study. Although the high-frequency component of the radiation force is nearly 2 MHz, the sampling frequency of the displacement waveform is 486 Hz (corresponding to the frame rate). Thus, an aliasing effect might be one of the reasons that the component is seen as a 100 Hz component.

As shown in Fig. 12(a), the displacement caused by ultrasonic actuation is attenuated during propagation. Also, in

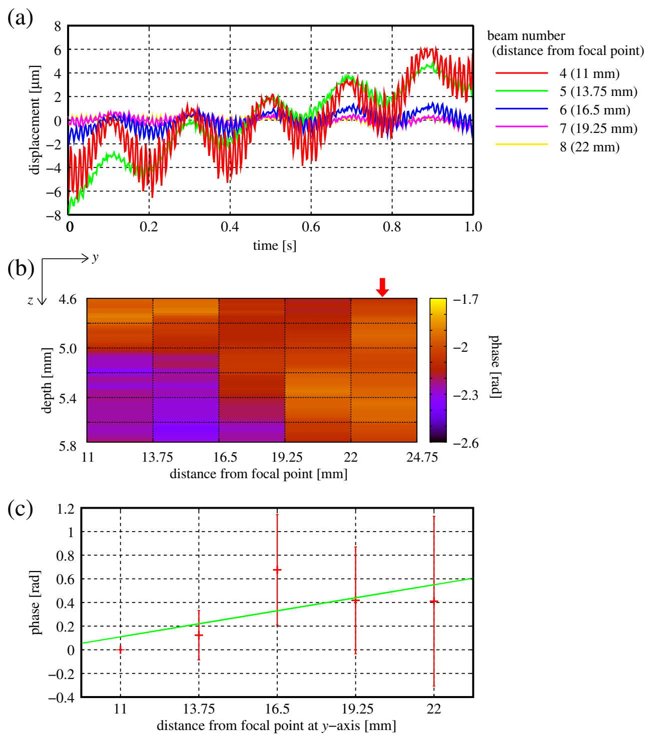

Fig. 12. (Color online) (a) Displacement waveforms, (b) spatial distribution of phases, and (c) average phases of displacements at Δf of 5 Hz obtained for porcine muscle phantom.

Figs. 12(b) and 12(c), phase delays due to the propagation of the shear wave are observed. The position of the analyzed region is indicated by the green square in Fig. 3. By determining the regression lines, as shown by the green line in Fig. 12(c), the shear wave propagation speed at Δf of 5 Hz was estimated using the slope of the regression line.

In Fig. 13, the shear wave propagation speeds are plotted as a function of the frequency difference Δf. By fitting the frequency characteristic of the shear wave propagation speed obtained using the Voigt model to the frequency characteristic measured by ultrasound, the viscoelastic constants of the porcine muscle tissue were estimated to be ($\mu_1^{\mathrm{p}} = 1.6\,\mathrm{kPa}$, $\mu_2^{\mathrm{p}} = 10.9\,\mathrm{Pa{\cdot}s}$), which were similar to the viscoelastic constants of cow muscle ($\mu_1 = 30$–$400\,\mathrm{kPa}$, $\mu_2 = 30$–$200\,\mathrm{Pa{\cdot}s}$),[25] beef muscle ($\mu_1 = 20\,\mathrm{kPa}$, $\mu_2 = 23\,\mathrm{Pa{\cdot}s}$),[26] and human muscle ($\mu_1 = 2.5\,\mathrm{kPa}$, $\mu_2 = 15\,\mathrm{Pa{\cdot}s}$)[27] reported in the literature. From these results, the proposed method could generate and measure the shear wave propagation and was also applicable to the estimation of the viscoelasticity of biological tissue.

4. Conclusions

In the present study, we actuated phantoms simulating soft biological tissue using dual acoustic radiation pressure and measured the propagation velocity of the generated shear wave as a function of the actuation frequency Δf. In polyurethane phantoms, the viscoelastic properties measured by ultrasound tend to be similar to those measured using a precision universal tester, though there were differences in their absolute values. Furthermore, an in vitro experiment using porcine abdominal muscle was conducted and the viscoelastic properties were also estimated as in the measurements of polyurethane phantoms. These results show the possibility of the proposed method for the noninvasive and quantitative assessment of the viscoelasticity of biological soft tissue.

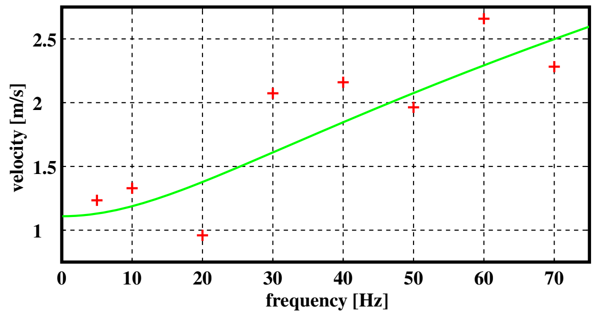

Fig. 13. (Color online) Shear wave propagation speeds in porcine muscle phantom plotted as a function of Δf. The solid line shows the frequency characteristic obtained using the Voigt model.

1) S. Shoji, *Kin Shikkan no Shindan to Chiryo* (Nagai Shoten, Osaka, 1988) p. 27 [in Japanese].
2) S. Sato and T. Inoue, *Byotai Seiri Bijuaru Mappu 4* (Igaku Shoin, Tokyo, 2010) p. 137 [in Japanese].
3) M. Fatemi, L. E. Wold, A. Alizod, and J. F. Greenleaf, IEEE Trans. Med. Imaging **21**, 1 (2002).
4) M. Fatemi and J. F. Greenleaf, Proc. Natl. Acad. Sci. U.S.A. **96**, 6603 (1999).
5) K. Nightingale, M. S. Soo, R. Nightingale, and G. Trahey, Ultrasound Med. Biol. **28**, 227 (2002).
6) G. E. Trahey, M. L. Palmeri, R. C. Bentley, and K. R. Nightingale, Ultrasound Med. Biol. **30**, 1163 (2004).
7) B. J. Fahey, K. R. Nightingale, R. C. Nelson, M. L. Palmeri, and G. E. Trahey, Ultrasound Med. Biol. **31**, 1185 (2005).
8) Japan Society of Ultrasonics in Medicine, Cho-onpa Igaku **11**, 41 (1984) [in Japanese].
9) J. Bercoff, M. Tanter, and M. Fink, IEEE Trans. Ultrason. Ferroelectr. Freq. Control **51**, 396 (2004).
10) K. Masuda, R. Nakamoto, N. Watarai, R. Koda, Y. Taguchi, T. Kozuka, Y. Miyamoto, T. Kakimoto, S. Enosawa, and T. Chiba, Jpn. J. Appl. Phys. **50**, 07HF11 (2011).
11) H. Hasegawa, M. Takahashi, Y. Nishio, and H. Kanai, Jpn. J. Appl. Phys. **45**, 4706 (2006).
12) Y. Odagiri, H. Hasegawa, and H. Kanai, Jpn. J. Appl. Phys. **47**, 4193 (2008).
13) Z. Wu, K. Hoyt, D. J. Rubens, and K. J. Parker, J. Acoust. Soc. Am. **120**, 535 (2006).
14) G. R. Torr, Am. J. Phys. **52**, 402 (1984).
15) A. J. Livett, F. W. Emery, and S. Leeman, J. Sound Vib. **76**, 1 (1981).
16) S. Catheline, J.-L. Gennisson, G. Delon, M. Fink, R. Sinkus, S. Abouelkaram, and J. Culioli, J. Acoust. Soc. Am. **116**, 3734 (2004).
17) Y. Yamakoshi, J. Sato, and T. Sato, IEEE Trans. Ultrason. Ferroelectr. Freq. Control **37**, 45 (1990).
18) H. Kanai, M. Sato, Y. Koiwa, and N. Chubachi, IEEE Trans. Ultrason. Ferroelectr. Freq. Control **43**, 791 (1996).
19) H. Kanai, H. Hasegawa, N. Chubachi, Y. Koiwa, and M. Tanaka, IEEE Trans. Ultrason. Ferroelectr. Freq. Control **44**, 752 (1997).
20) H. Kanai, K. Sugimura, Y. Koiwa, and Y. Tsukahara, Electron. Lett. **35**, 949 (1999).
21) K. Ikeshita, H. Hasegawa, and H. Kanai, Jpn. J. Appl. Phys. **51**, 07GF14 (2012).
22) K. Kitamura, H. Hasegawa, and H. Kanai, Jpn. J. Appl. Phys. **51**, 07GF08 (2012).
23) Y. Honjo, H. Hasegawa, and H. Kanai, Jpn. J. Appl. Phys. **51**, 07GF06 (2012).
24) H. Shida, H. Hasegawa, and H. Kanai, Jpn. J. Appl. Phys. **51**, 07GF05 (2012).
25) S. Catheline, F. Wu, and M. A. Fink, J. Acoust. Soc. Am. **105**, 2941 (1999).
26) E. R. Fitzgerald, E. Ackerman, and J. W. Fitzgerald, J. Acoust. Soc. Am. **29**, 61 (1957).
27) H. L. Oestreicher, J. Acoust. Soc. Am. **23**, 707 (1951).